Available online at www.sciencedirect.com
SCIENCE DIRECT®
Chemical Physics 286 (2003) 277–291
Chemical Physics
www.elsevier.com/locate/chemphys

Excited-state absorption dynamics in polymethine dyes detected by polarization-resolved pump–probe measurements

Richard S. Lepkowicz[a,*], Olga V. Przhonska[a,b], Joel M. Hales[a], David J. Hagan[a], Eric W. Van Stryland[a], Mikhail V. Bondar[b], Yuriy L. Slominsky[c], Alexei D. Kachkovski[c]

[a] *School of Optics/CREOL (Center for Research and Education in Optics and Lasers), University of Central Florida, Orlando, FL 32816-2700, USA*
[b] *Institute of Physics, National Academy of Sciences, Prospect Nauki 46, Kiev-28, 03028, Ukraine*
[c] *Institute of Organic Chemistry, National Academy of Sciences, Murmanskaya str. 5, Kiev-94, 02094, Ukraine*

Received 24 May 2002

Abstract

Polarization-resolved excitation-probe measurements are performed for a new series of polymethine dyes in several solvents and a polyurethane acrylate elastopolymer. We describe our experimental studies and give an analysis of the nature of the rotational motions of excited molecules and orientation of the excited-state transitions relative to transitions from the ground state.

Keywords: Excited-state absorption; Polymethine dye; Rotational motion; Orientation of transition dipole moments; Anisotropy

1. Introduction

Polymethine dyes (PDs) in liquid solutions and polymeric media have been extensively studied as promising materials for laser and optoelectronic applications. These studies led to the development of several series of PDs that exhibit strong excited-state absorption (ESA) in the visible, with excited-state cross-sections as large as 7×10^{-16} cm^2 which is comparable to that of the ground state [1]. The most extensive information about ESA in PDs is currently presented in [2–4]. In our previous paper [4] we reported the prediction and observation of two additional ESA bands in the near infrared region, and also proposed the transition modeling based on a study of the steady-state excitation anisotropy and quantum-chemical calculations. Analyzing the theoretical predictions and experimental data we concluded that the most intense

* Corresponding author. Tel.: +407-823-6865; fax: +407-823-6880.
E-mail address: rlepkowi@mail.ucf.edu (R.S. Lepkowicz).

0301-0104/03/$ - see front matter
PII: S0301-0104(02)00937-0

ESA broadband spectrum in the visible is connected with the $S_1 \rightarrow S_5$ transition. It should be noted at this time that under current quantum-chemical theories the $S_1 \rightarrow S_5$ transition would be forbidden. This issue is discussed in Section 4.2. Two other bands are connected with the much less intense $S_1 \rightarrow S_2$ and $S_1 \rightarrow S_4$ allowed transitions. The $S_1 \rightarrow S_3$ transition is probably forbidden and was not observed experimentally. The orientation of the dipole moment for the ESA transitions and their intensities has not been investigated as thoroughly. In [5,6] the orientations of the transition dipole moment for the ESA band in oxazine dyes (Acridine Orange, Nile Blue and Cresyl Violet) and Rhodamine 6G were measured with a picosecond pump–probe technique. In all cases the ESA transition moments and ground-state absorption $S_0 \rightarrow S_1$ dipoles were found to be parallel. To our knowledge, these measurements and their analysis for PDs have yet to be performed. This is one of the goals of the current paper.

In this paper we also continue our investigation of the excited-state dynamics and molecular motions in different micromolecular environments started in [7]. It should be noted that picosecond pump–probe methods have been extensively used to measure ground and excited-state dynamics since the 1970s [8–10]. In our previous paper [7] we proposed to use a time-resolved induced anisotropy method to obtain more direct information about molecular motions.

Thus in this paper we describe experimental studies and give the analysis for a new series of PD molecules that aid in the understanding of the:

1. Nature of the rotational motions of excited molecules in several host materials.
2. Orientation of the ESA transitions between the $S_0 \rightarrow S_n$ $(n = 1, 2, 3, \ldots)$ and the fluorescence emission dipole moment $S_1 \rightarrow S_0$.
3. Orientation of the ESA transitions between the $S_0 \rightarrow S_n$ $(n = 1, 2, 3, \ldots)$ and the excited state transition dipole moments $S_1 \rightarrow S_n$ $(n = 2, 3, 4, \ldots)$.

The experimental techniques used to investigate the PD molecules are:

1. Linear absorption spectral measurements.
2. Steady-state excitation anisotropy measurements.
3. Picosecond polarization-resolved pump–probe measurements.
4. Femtosecond polarization-resolved pump–probe measurements.

The analysis includes:

1. Molecular volume calculations in van der Waals model using the HyperChem software package.
2. Numerical fitting of the pump–probe measurements.

2. Experimental

2.1. Materials

The molecular structures of the dyes studied in this paper are shown in Fig. 1. Their chemical names are: 2-[5-(1,3-dihydro-3,3-dimethyl-1-propyl-2H-indol-2-ylidene)-1,3-pentadienyl]-3,3-dimethyl-1-propylindolium iodide (labeled as PD 2350); 2-[5-(1,3-dihydro-3,3-dimethyl-1-propyl-2H-indol-2-ylidene)-3-cyano-1,3-pentadienyl]-3,3-dimethyl-1-propylindolium iodide (labeled as PD 2351); 2-[2-[3-[(1,3-dihydro-1,3,3-trimethyl-5-phenyl-2H-indol-2-ylidene)ethylidene]-5-methyl-2-(4-methoxyphenyl)-1-cyclohexen-1-yl]ethenyl]-1,3,3-trimethyl-5-phenylindolium tetrafluoroborate (labeled as PD 2335); 2-[2-[3-[(1,3-dihydro-1,3,3-trimethyl-5-phenyl-2H-indol-2-ylidene)ethylidene]-2-phenyl-1-cyclohexen-1-yl]ethenyl]-1,3,3-trimethyl-5-phenylindolium tetrafluoroborate (labeled as PD 2338); 2-[9-(1,3-dihydro-1,3,3-trimethyl-2H-indol-2-ylidene)-3,7-dimethyl-4,6-(2,2-dimethyltrimethylene)-1,3,5,7-nonatetraenyl]-1,3,3-trimethylindolium perchlorate (labeled as PD 824); 2-[9-(1-ethyl-3,3-dimethyl-2H-benzo[e]indol-2-ylidene)-3,7-dimethyl-4,6-(2,2-dimethyltrimethylene)-1,3,5,7-nonatetraenyl]-1-ethyl-3,3-dimethylbenzo[e]indolium perchlorate (labeled as PD 2332) and 2-[3-(1-butyl-6-butoxybenz[c,d]-indol-2-ylidene)-1-propenyl]-1-butul-6- butoxybenz-[c,d]indolium tetrafluoroborate (labeled as PD 2257). These PDs were synthesized at the Institute of Organic Chemistry, Kiev, Ukraine. Their molecular structures were confirmed by elemental analysis and nuclear magnetic resonance spectra. Specific synthesis for PDs 824 and 2332 was described in [11], the synthesis of the other dyes was

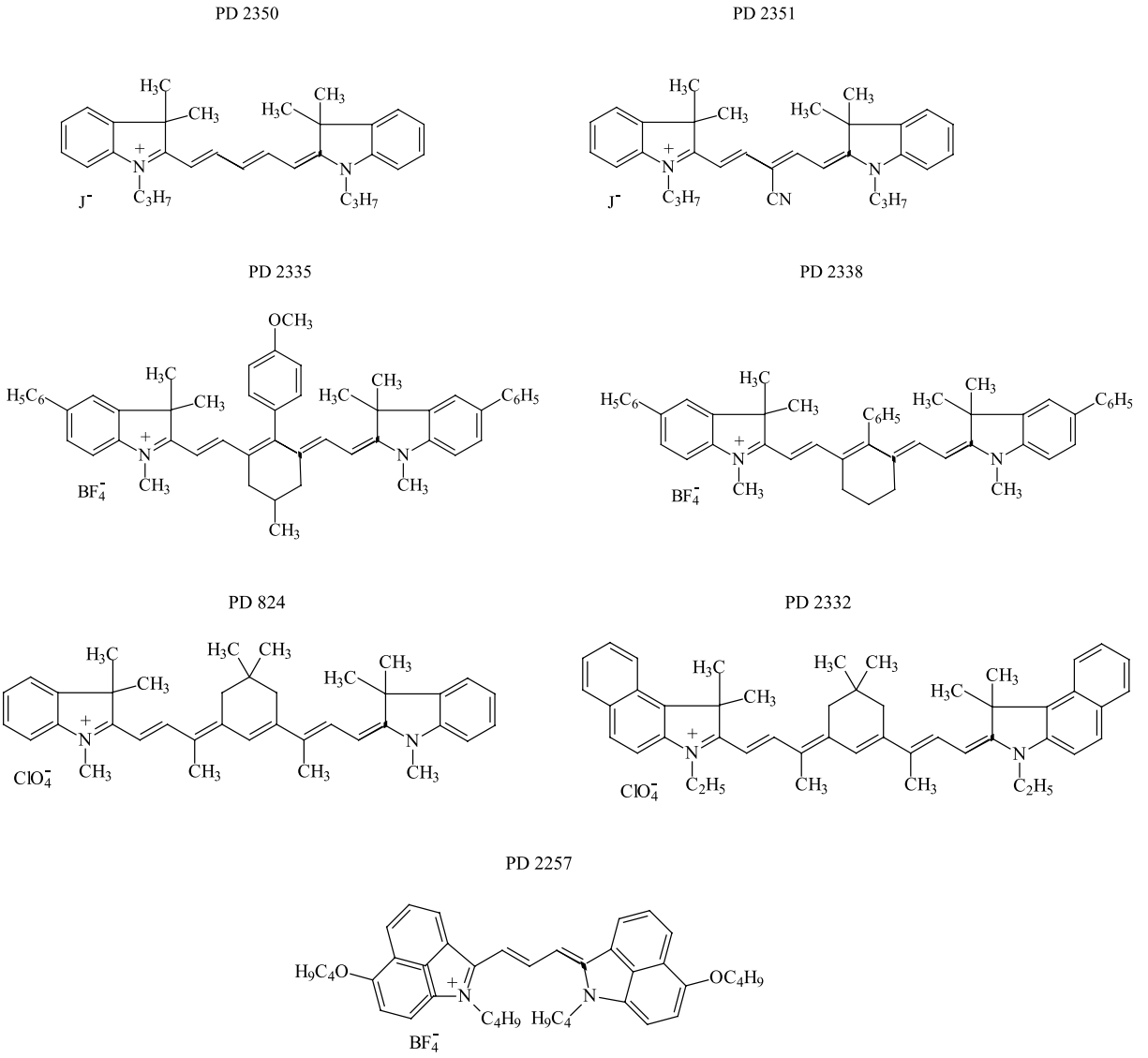

Fig. 1. Molecular structures.

performed by standard methods described in [12,13]. These dyes were chosen based on their photophysical and nonlinear optical properties, particularly their large ESA that is favorable for passive optical limiting [1].

The experiments were performed in several solvents of different viscosity and polarity: absolute ethanol, ethylene glycol and methylene chloride as well as in the polymeric medium, polyurethane acrylate (PUA). The polymeric samples were prepared using the previously reported radical photopolymerization procedure [1,14]. The linear absorption spectra of all dyes in ethanol, presented in Fig. 2, were recorded with a Varian Cary 500 spectrophotometer.

The spectroscopic and nonlinear absorption properties of PDs are determined mainly by the existence of a delocalized π-electron system in the polymethine chromophore (or polymethine chain) and the symmetric terminal groups. First of all, the

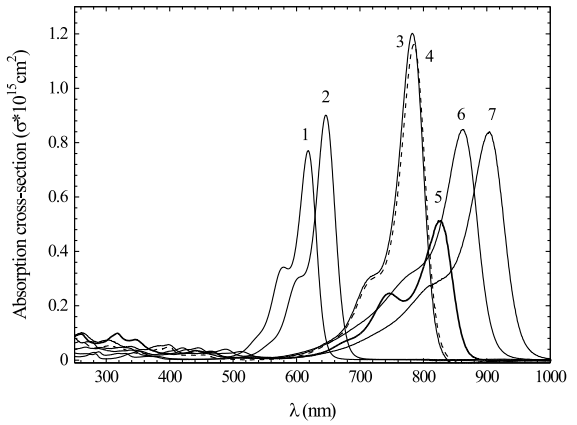

Fig. 2. Linear absorption spectra for PD 2351 (1), PD 2350 (2), PD 2335 (3), PD 2338 (4), PD 2257 (5), PD 824 (6) and PD 2332 (7) in ethanol.

dyes differ by the length of the polymethine chain: di- (PDs 2350 and 2351), tri- (PDs 2335 and 2338) and tetracarbocyanines (PDs 824 and 2332). It is well known that an increase in the length of the polymethine chain by one double bond with the same terminal groups leads to a red shift of the absorption maximum of about 100 nm. The dyes PD 2351 and 2350 with the shortest polymethine chain absorb at 618 and 646 nm (absorption peaks), respectively. The long tails near the nitrogen atoms increase the solubility of the dyes and prevent the formation of aggregates even at large concentration up to 3×10^{-3} M. The blue shift of the absorption maximum for PD 2351, as compared to the unsubstituted PD 2350, is connected with the influence of CN-acceptor group incorporated into the mesoposition of the polymethine chain. The absorption maxima of the tricarbocyanine PDs, 2335 and 2338, are shifted into the red to 782 and 784 nm, respectively, and are characterized by the largest (within this series of PDs) ground-state absorption cross-sections ($\sigma_g = 1.2 \times 10^{-15}$ cm^2). They differ from the dicarbocyanines not only by the length and the substitutes in the chain, but also by the structure of the terminal groups. In particular the structure of the terminal groups determines a larger red shift of about 140 nm compared to the dicarbocyanine dyes. A decrease in σ_g has been observed for the tetracarbocyanine PDs 824 and 2332. Their absorption maxima are placed at 861 and 904 nm, respectively, and their absorption bands are broader than for the tricarbocyanines. PD 2332 is characterized by the longest π-electron system in the terminal groups, which explains its long wavelength spectral position. The absorption band for PD 2257 is placed between the tri- and tetracarbocyanines despite the fact that its polymethine chromophore includes only one double bond. PD 2257 and its analogues were proposed as an alternative way for the synthesis of long wavelength absorbing dyes with a relatively short polymethine chain, and therefore having increased photochemical stability [13]. This type of dye has been used as a saturable absorber for picosecond lasers [15].

2.2. Experimental methods

2.2.1. Fluorescence excitation anisotropy measurements

Steady-state fluorescence spectra (using low concentration $\sim 10^{-6}$ M/l liquid dye solutions to avoid reabsorption) as well as anisotropy excitation spectra (using high viscosity solvents to avoid reorientations) were obtained with a PTI Quantamaster Spectrofluorimeter. Excitation anisotropy measurements give us information about the spectral position and orientation of the transition dipole moments from the ground to first and higher excited states $S_0 \rightarrow S_n$ $(n = 1, 2, 3, \ldots)$ relative to the emission dipole moment orientation. The excitation anisotropy spectrum, $R(\lambda)$, was calculated as a function of the excitation wavelength λ at a fixed emission wavelength (usually near a fluorescence maximum) after appropriate background subtraction on each component. $R(\lambda)$ is defined as

$$R(\lambda) = \frac{I_{vv}(\lambda) - G(\lambda) I_{vh}(\lambda)}{I_{vv}(\lambda) + 2G(\lambda) I_{vh}(\lambda)}, \tag{1}$$

where $G(\lambda) = I_{hv}(\lambda)/I_{hh}(\lambda)$ and $I_{vv}(\lambda)$, $I_{hv}(\lambda)$, $I_{vh}(\lambda)$ and $I_{hh}(\lambda)$ are the polarized fluorescence intensities at the excitation wavelength λ. The first and second subscripts refer to the orientation (v for vertical and h for horizontal) of the emission and excitation polarizations, respectively [16]. The angle between the absorption and emission tran-

sition moments can be determined from the anisotropy $R(\lambda)$ by

$$R = \frac{2}{5}\left(\frac{3\cos^2(\beta) - 1}{2}\right), \quad (2)$$

where β is the angle between the absorption transition moment and the emission transition moment [16]. The results of the steady-state excitation anisotropy measurements are presented below.

2.2.2. Picosecond polarization-resolved pump–probe measurements

These measurements were conducted using a frequency doubled (532 nm), active/passive modelocked, 10 Hz repetition rate, Nd:YAG laser. The laser produces a pulse train, from which a single 25 ps (FWHM) pulse is switched out for the measurements. The basic experimental set-up is shown in Fig. 3. The pump and probe beams are generated from the same laser and are separated with a beam splitter with the majority of the energy going into the pump beam and only a small percentage (at least 200 times less) going into the probe beam. The energy range of the pump beam was 0.2–7 μJ. The pump and probe beams are focused to waists of radius 100 and 18 μm (half width $1/e^2$ maximum), respectively. The pump beam should be larger than the probe beam to ensure that the probe beam senses a uniform excitation region in the sample. The pump irradiance was at least an order of magnitude larger than that of the probe (except in the case of PD 2350 where the ratio was 7). The probe beam could be temporally delayed with respect to the pump beam up to 7 ns and its irradiance was kept low, so as not to induce any nonlinearity in the sample. The pump and the probe beams are overlapped at a small angle (~5°) within the sample so the probe beam can be separated after the sample from the pump as shown in Fig. 3. The polarization of the probe is fixed and a polarizer placed after the sample is aligned parallel with the probe polarization. The pump polarization is adjusted with a half-wave plate and can be set to any angle (α) with respect to the probe polarization. The probe beam is monitored before and after the sample using large area silicon photodiodes.

In this type of experiment it is very important to know the position of zero delay. This is done by performing a pump–probe experiment using CS_2, which, due to its finite relaxation time and the fact that the laser pulses are slightly chirped, produces a two-beam coupling effect in the sample that allows us to easily determine zero delay [17].

2.2.3. Femtosecond polarization-resolved pump–probe measurements

The laser system used for these experiments was a Clark-MXR 2001 Ti:sapphire amplified frequency-doubled erbium-doped fiber ring oscillator system followed by two optical parametric generator/amplifiers OPA (Light Conversion, model TOPAS), providing 100–120 fs (FWHM) with independently tunable wavelengths from 0.55 to 2.2 μm. The general experimental set-up is shown in Fig. 3. A more detailed description of this experiment can be found in [4]. The pump beam was either the output of the OPA which has pulse

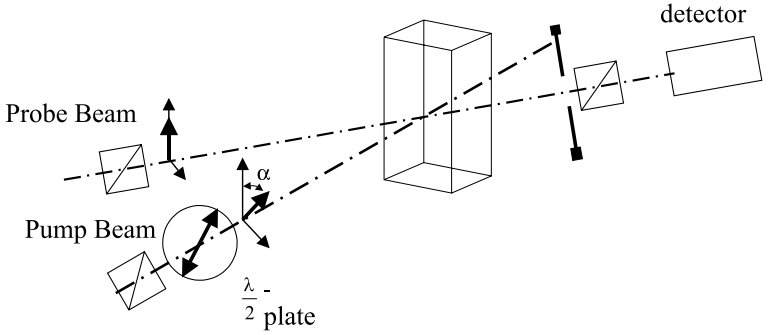

Fig. 3. Schematic of general pump–probe set-up to describe both picosecond and femtosecond measurements.

energies of tens of microjoules or the output of the Clark-MXR 2001 directly (775 nm) or its second harmonic (388 nm). The probe beam was either the output of the OPA or a subpicosecond white-light continuum (WLC), generated by focusing a 1 μJ pulse from an OPA at a wavelength of 1400 nm into a 2-mm thick sapphire plate [18]. Depending on the probe wavelength used, two different detection systems were used. In the visible region, large area Si photodiodes were used with narrow-band filters with a bandwidth of 10 nm to select a portion of the transmitted WLC probe beam. At wavelengths longer than 1000 nm the probe beam was derived directly from the OPA and was detected with germanium photodiode detectors. The probe can be delayed with respect to the pump beam up to 1 ns, which is not sufficient to measure excited state or reorientation decay times, but the purpose of these experiments was to measure the nonlinear transmittance as a function of the relative polarization of pump and probe. These experiments were carried out for fixed delays of 0.6 and 30 ps.

3. Results

3.1. Excitation anisotropy measurements and absorption $S_0 \rightarrow S_n$

It is well known that the absorption spectra in the visible and near IR region for PDs are characterized by a strong single band, $S_0 \rightarrow S_1$, with a typical FWHM = (750–950) cm^{-1} – see Fig. 2. A small vibrational maximum due to carbon–carbon deformational vibrations is situated about 1200 cm^{-1} above the main absorption peak. The absorption spectra in the short wavelength region are characterized by small intensity and strongly overlapped bands, which correspond to transitions

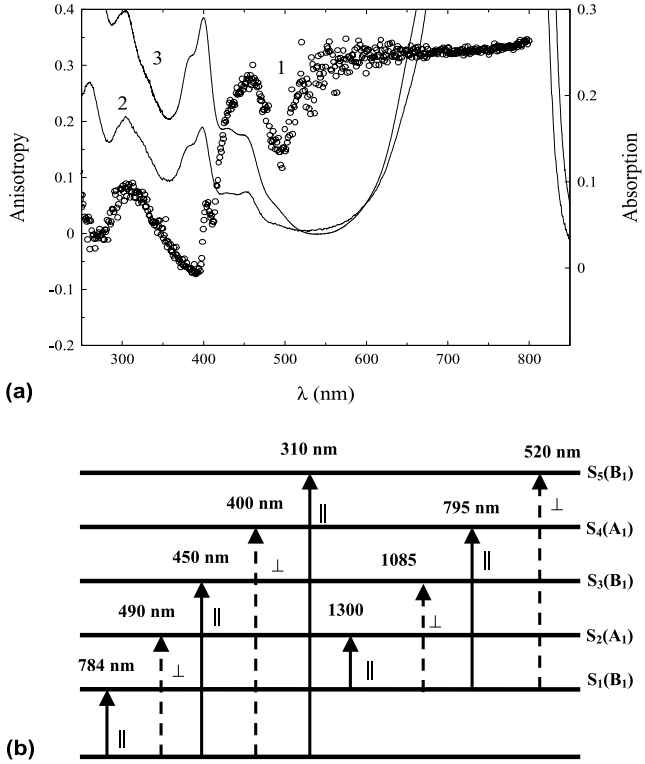

Fig. 4. (a) Excitation anisotropy, left axis *y*, (1) and linear absorption spectra, right axis *y*, in ethanol (2) and glycerol (3) for PD 2338; (b) simplified transition modeling for PD 2338.

from the ground to the higher excited states. In order to distinguish between different $S_0 \rightarrow S_n$ $(n = 2, 3, \ldots)$ transitions, we performed excitation anisotropy measurements. In these measurements, the fluorescence intensity near the peak fluorescence wavelength, resolved into components parallel ($I_\parallel$) and perpendicular ($I_\perp$) to the excitation polarization, was measured as a function of excitation wavelength (λ). The steady-state anisotropy excitation spectra, $R(\lambda)$ for PD 2338 and PD 2335 in glycerol are presented in Figs. 4(a) and 5(a). Measurements in ethanol show the same positions in anisotropy peaks but with smaller anisotropy values (maximum 0.06–0.07) due to the fast reorientation times that depolarize the fluorescence. In high viscosity glycerol solutions the rate of reorientational motions in the excited state is much slower than in ethanol and anisotropy values within the first absorption band are high and close to the theoretical limit of 0.4 [16].

The results for the location of the excited-state energy levels, maximum anisotropy, and the orientation of the transition dipole moments from Figs. 4(a) and 5(a) are summarized in Table 1. The main results being that both dyes have a similar energy level structure with the largest transition

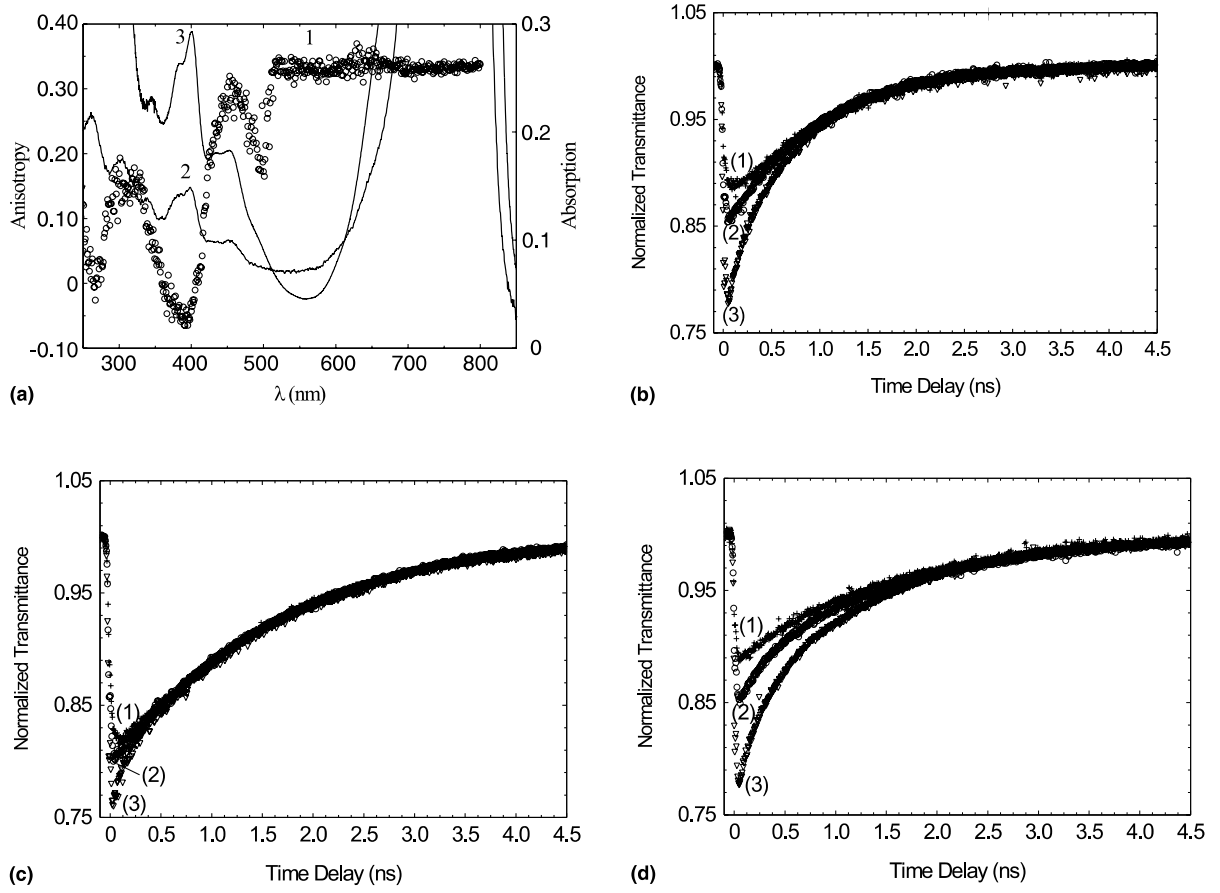

Fig. 5. (a) Steady-state excitation anisotropy, left axis y, (1) and linear absorption spectra, right axis y, in ethanol (2) and glycerol (3) for PD 2335. (b) Pump–probe results for PD 2335 in ethanol for the pump polarization perpendicular (1), at the magic angle (2) and parallel (3). (c) Pump–probe results for PD 2335 in methylene chloride for the pump polarization perpendicular (1), at the magic angle (2) and parallel (3). (d) Pump–probe results for PD 2335 in PUA for the pump polarization perpendicular (1), at the magic angle (2) and parallel (3).

Table 1
Results for the steady-state fluorescence anisotropy measurements for PD 2338 and PD 2335

Energy transition	Spectral peak of anisotropy (nm)	Maximum anisotropy	Transition moment orientation (°)
PD 2338			
$S_0 \rightarrow S_2$	490	0.12–0.16	39–43
$S_0 \rightarrow S_3$	450	0.26–0.29	25–29
$S_0 \rightarrow S_4$	410	−0.05–−0.08	60–63
$S_0 \rightarrow S_5$	310	0.06–0.1	45–49
PD 2335			
$S_0 \rightarrow S_2$	500	0.16–0.20	35–40
$S_0 \rightarrow S_3$	450	0.27–0.31	23–28
$S_0 \rightarrow S_4$	390	−0.04–−0.07	59–63
$S_0 \rightarrow S_5$	310	0.12–0.18	37–43

The spectral peak of anisotropy gives the location of the excited-state energy levels. The maximum anisotropy refers to the anisotropy at the peak spectral position. The transition moment orientation (β) is relative to the emission dipole moment and is calculated using the maximum anisotropy and Eq. (2).

dipole moment angle associated with the $S_0 \rightarrow S_4$ transition (59–63° relative to the $S_0 \rightarrow S_1$ transition dipole) and the smallest the $S_0 \rightarrow S_3$ (23–29°) transition. For comparison, the absorbance is plotted together with the anisotropy in Figs. 4(a) and 5(a). There is a correlation between the position of the $S_0 \rightarrow S_n$ transitions found from the anisotropy excitation spectrum and the position of the short wavelength absorption bands for both dyes. For example, PD 2338 has a low intensity shoulder in the absorption spectrum near 490 nm that may be connected with the $S_0 \rightarrow S_2$ transition. More intensive bands around 450 and 400 nm relate to $S_0 \rightarrow S_3$ and $S_0 \rightarrow S_4$ transitions.

The next step of this investigation was to estimate the position of the $S_1 \rightarrow S_n$ ($n = 2, 3$ and higher) transitions using a methodology based on steady-state anisotropy measurements and quantum-chemical calculations as described in [4] for similar dyes. As an example of this modeling, the results for transitions in PD 2338 are presented in Fig. 4(b). Excited-state absorption bands $S_1 \rightarrow S_2$ and $S_1 \rightarrow S_5$ were observed experimentally as described in [4].

3.2. Pump–probe polarization data

To further our understanding of the nature of ESA in these dyes we have undertaken a detailed investigation of their excited-state dynamics using the polarization-resolved pump–probe technique. This method creates an anisotropic distribution of molecules due to the linear polarization of the pump beam and the angular dependence of the absorption transition moments in the molecule. Using this technique, not only can the lifetime decay kinetics be separated from the rotational motion of the molecule, but we can also determine the orientation of the excited-state transition moments. Since this method has been extensively used in the past [8–10] and was described in detail in our previous paper [7], only a brief review will be given.

In the pump–probe experiment an intense linearly polarized pump beam induces a nonlinear response in the medium that is then sensed by a time delayed weak probe beam. The change in transmittance (ΔT) of the probe beam has been shown [8] to be proportional to the excited-state population density, provided ΔT is small. Even for the largest transmittance change ($\sim$30%) observed in our data, the errors in lifetime and reorientation time measurements as determined from the decay in ΔT are never more than $\sim$10%.

By conducting experiments in which the probe polarization is set parallel, perpendicular and at the magic angle (54.7°) to the pump beam, the excited-state decay time (τ_F) can be separated from the reorientation relaxation time (τ_R). The results for the normalized transmittance versus time delay for several PDs in different media are shown in Figs. 5–7. Figs. 5(b–d) and 6(a–c) show

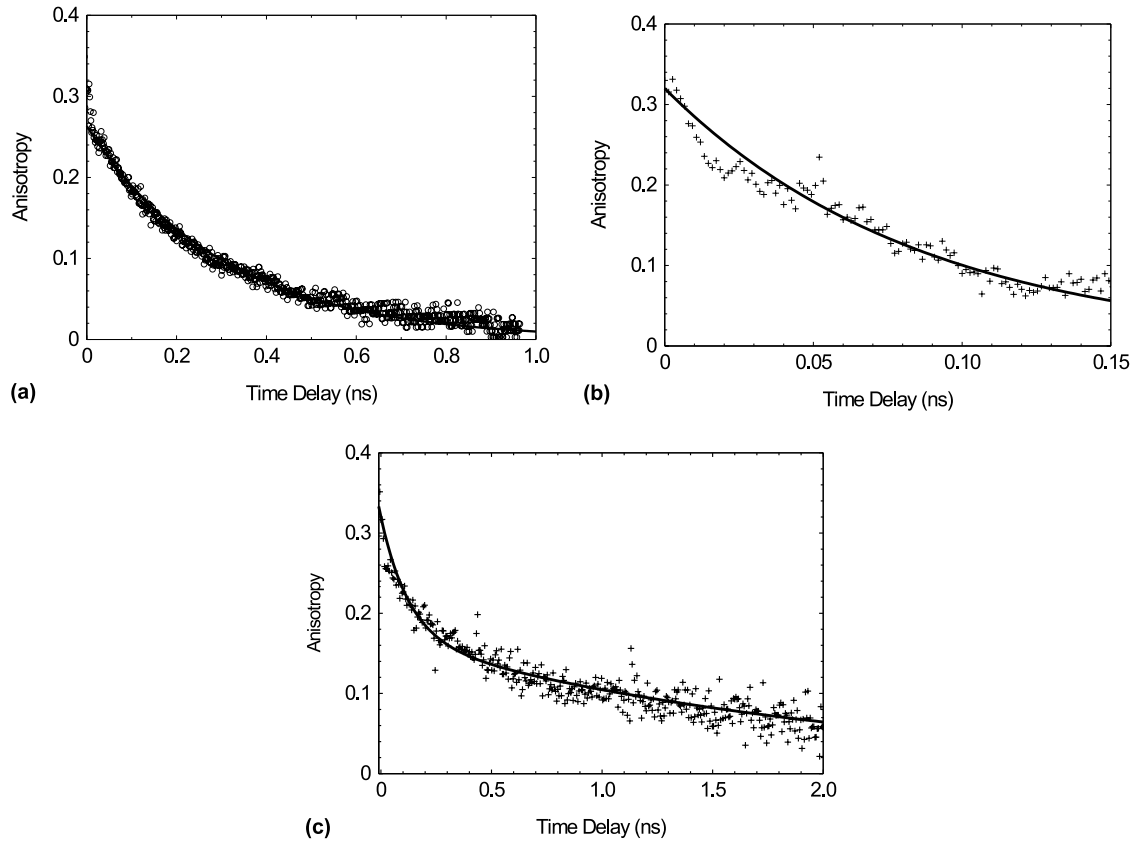

Fig. 6. (a) Anisotropy results with best-fit curve for PD 2335 in ethanol. (b) Anisotropy results with best-fit curve for PD 2335 in methylene chloride. (c) Anisotropy results with best-fit curve for PD 2335 in PUA.

the experimental data for PD 2335 in ethanol, methylene chloride and PUA. Fig. 7(a–c) shows the data for PD 2351 in ethanol. The change in transmittance of the parallel $\Delta T_{\parallel}(t)$ and perpendicular $\Delta T_{\perp}(t)$ measurements can be used to define the anisotropy $R(t)$, which gives the rotational reorientation time τ_R as

$$R(t) = [\Delta T_{\parallel}(t) - \Delta T_{\perp}(t)]/[\Delta T_{\parallel}(t) + 2\Delta T_{\perp}(t)] = R\exp(-t/\tau_R), \quad (3)$$

where R is given by Eq. (2), but β now refers to the angle between the pump absorption transition moment and the probe absorption transition moment. The anisotropy curves in different media for PDs 2335 and 2351 are shown in Figs. 6(a–c) and 7(c), respectively.

Thus from the magic angle and anisotropy curves we can determine the excited-state decay time τ_F, the rotation time τ_R, and the maximum anisotropy, R. The values of τ_F and τ_R for all the dyes investigated are presented in Table 2 and the analysis of these results is given in the following section. Determination of R usually becomes complicated by the influence of the coherent beam-coupling effect [17]. More accurate values of R can be obtained with the short time delay pump–probe measurements taking special care to determine the zero delay position as described previously in Section 2.2.2. These data are shown in Table 3.

A more detailed investigation of the orientation of the ESA transition moments was performed by measuring the transmission of the probe beam at a fixed time delay as a function of the angle between

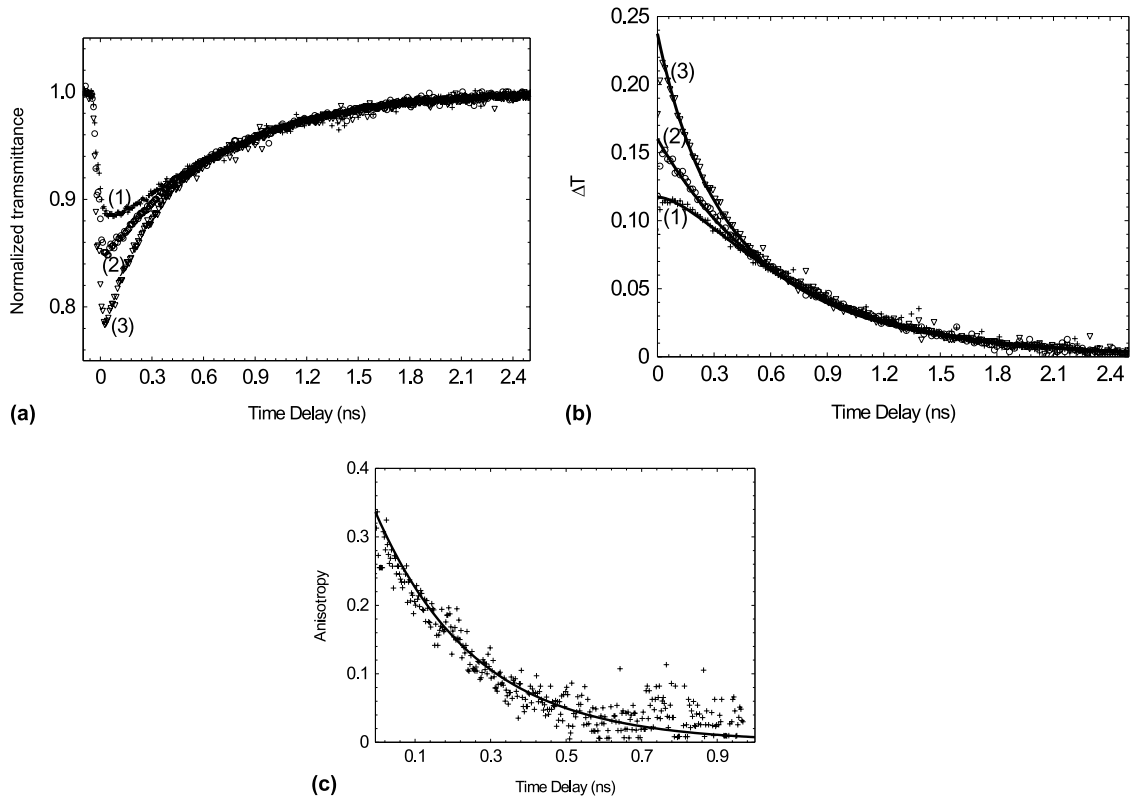

Fig. 7. (a) Results for PD 2351 in ethanol: normalized probe transmittance for pump polarization perpendicular (1), magic angle (2), and parallel (3) with respect to the probe beam. (b) Results for PD 2351 in ethanol: change in transmittance (ΔT) with best fits for pump polarization perpendicular (1), magic angle (2) and parallel (3) with respect to the probe beam. (c) Results for PD 2351 in ethanol: anisotropy data with best fit.

the pump and probe polarization. Using this technique with a tunable femtosecond laser system as described in Section 2.2.3 it is possible to determine the orientations of all the transition moments in the molecule. These results for PD 2338 in ethanol are shown in Fig. 8(a,b) and they are discussed in the following section.

4. Discussion

4.1. Excited-state dynamics

To study the nature of rotational motions in the excited states of PDs, we performed polarization-resolved pump–probe measurements in several solvents of different viscosity (η) and polarity as well in the polymeric medium PUA. The polarity of the solvents can be characterized by their orientational polarizability, which is given by

$$\Delta f = (\varepsilon - 1)/(2\varepsilon + 1) - (n^2 - 1)/(2n^2 + 1), \qquad (4)$$

where ε is the static dielectric constant and n is the refractive index of the solvent [16]. The values for η and Δf are shown in Table 2.

The anisotropy decay for all the dyes in liquid solvents is found to be monoexponential with decay times τ_R shown in Table 2. The largest lifetime values of 1300–1560 ps were obtained for the dyes in PUA and methylene chloride. Reorientation times in ethanol are in the range of 200–650 ps; in ethylene glycol: 2100–2700 ps and in methylene chloride ~75 ps (the shortest τ_R). No correlation was found between the rotational reorientation

Table 2
Calculated (τ_R^C) and experimental (τ_R) characteristics of rotation times in different media: ethanol (ETH), ethylene glycol (ETG), methylene chloride (MLC) and PUA

Dye	Solvent	η (mPa s)	Δf	T_L	C ($\times 10^4$) (M)	τ_F (ps)	τ_R (ps)	τ_R^C (ps)	V (Å)	m
824	ETH	1.074	0.29	0.83	1	145	330	130	490	12
824	ETG	16.1	0.27	0.8	1	140	2100	2000	490	0–1
2257	ETH	1.074	0.29	0.87	3	40	–	150	550	–
2350	ETH	1.074	0.29	0.81	2	800	200	100	390	6
2350	ETG	16.1	0.27	0.81	1.7	1200	–	1600	390	–
2351	ETH	1.074	0.29	0.79	0.5	660	260	110	400	9
2351	ETG	16.1	0.27	0.78	0.5	760	2700	1600	400	4
2332	ETH	1.074	0.29	0.71	3.5	110	650	150	570	30
2332	ETG	16.1	0.27	0.71	3.5	90	–	2300	570	–
2335	ETH	1.074	0.29	0.88	3	880	300	165	620	10
2335	PUA	–	–	0.78	5	1500	130 2600	–	620	–
2335	MCL	0.413	0.21	0.82	4	1560	85	65	620	2
2338	PUA	–	–	0.78	25	1300	200 2100	–	580	–
2338	ETH	1.074	0.29	0.88	12	900	400	160	580	15

η and Δf are parameters of the solvent (viscosity and orientation polarizability). T_L and C are experimental values of linear transmittance and concentration. Sample thickness is 1 mm. V and m are calculated molecular volume and number of the solvent molecules in the shell. The error bars were estimated as 10% for τ_F and 15% for τ_R.

time and the viscosity of the solvents. To get a basic understanding of this discrepancy we used the simplest possible model, which is the Stokes–Einstein–Debye (SED) model, and PD molecular volumes calculated using the HyperChem software package [7] to predict the rotational reorientation time. The SED model relates the rotational correlation time to the molecular and solvent parameters as:

$$\tau_R^C = \eta V/kT, \tag{5}$$

where V is the molecular volume of the rotating units, k is the Boltzmann constant and T is the temperature. As can be seen from Table 2, all calculated τ_R^C in ethanol are 2–3 times less than the measured τ_R, meaning that the actual volumes of the rotating unit are much larger than the corresponding van der Waals volumes. This difference may be attributed to the interaction between the dye and solvent leading to the formation of a solvent shell.

In Table 2 we put a calculated number of solvent molecules (m) forming the surrounding solvent shell. The ethanol corresponds to a "stick" rotation condition [16] with the number of molecules forming the solvent shell ranging from 6 to 30. PD 2335 in methylene chloride corresponds to more of a "slip" rotation condition [16].

Anisotropy decay in PUA is described by two quite different exponential decay times. The coexistence of two different decays may be explained by the restriction of the fast decay process (190–200 ps) in the polymer leading to only partial depo-

Table 3
Maximum anisotropy values R and calculated angles between transition dipole moments β for PDs in different media: ethanol (ETH), ethylene glycol (ETG), methylene chloride (MLC) and PUA

Dye	Solvent	R	β
824	ETH	0.22	33
824	ETG	0.25	30
2257	ETH	0.26	29
2350	ETH	0.38	10
2350	ETG	0.4	0
2351	ETH	0.34	18
2351	ETG	0.4	0
2332	ETH	0.3	24
2332	ETG	0.28	26
2335	ETH	0.32	20
2335	PUA	0.35	17
2335	MCL	0.33	20
2338	PUA	0.32	21
2338	ETH	0.34	18

The error bars were estimated as 15%.

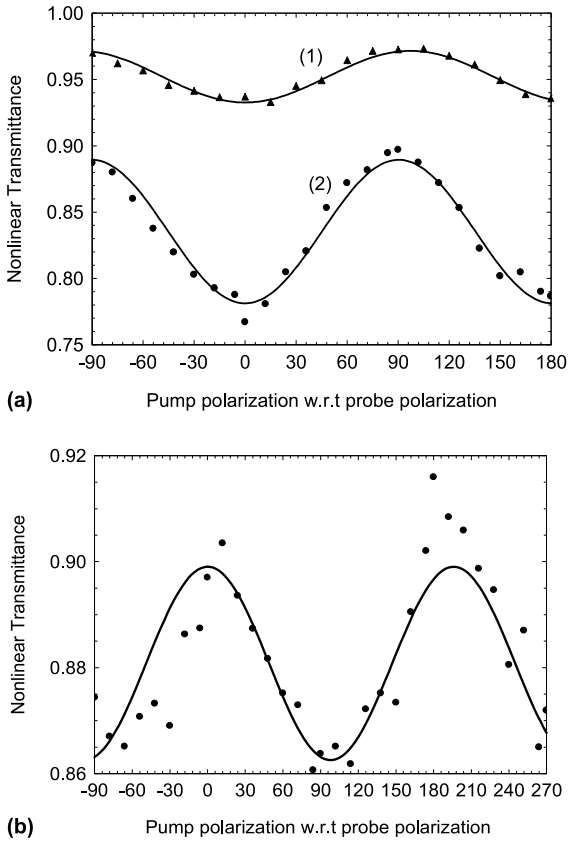

Fig. 8. Femtosecond pump–probe results for PD 2338 for (a) excitation with 640 nm into S_1 and probing with 1300 nm (1) into S_2 and probe with 532 nm (2) into S_5; (b) excite with 388 nm into S_4 and probe with 532 nm into S_5 after ultrafast S_4–S_1 relaxation.

larization of the excited state. Complete loss of anisotropy was observed as a result of the slower decay process (2100–2600 ps). In our previous paper [7] we reported the results on rotational motions in PUA for PD 2093 and a squarylium dye SD 2243. We proposed an explanation based on the formation of microcavities of free volume due to the photopolymerization process. The fast rotational component may be connected with the rotation of molecular fragments, which are limited by the free volume of the microcavities. The slower rotational component is probably connected with the rotation of the entire molecule. Due to the viscoelastic properties of PUA (glass transition temperature is ~ -50 °C) this material at room temperature is characterized by a faster segmental dynamics and microscale fluctuations of density compared to the glassy state. From our experimental results we can conclude that complete depolarization in the nanosecond time scale is a property of the highly elastic state of the polymeric host. Therefore, the polarization-resolved pump–probe technique may be successfully used to study the microstructure and microviscosity of polymeric materials. We will continue our studies in this direction.

4.2. ESA orientations

The orientation of the $S_1 \rightarrow S_n$ ($n = 2, 3$ and higher) transition moments is connected to the maximum anisotropy value R, from which the angle β can be calculated as described in Section 3.2. These values for all the PDs studied are presented in Table 3. One of our goals is to compare the excited-state transition moment orientations ($S_1 \rightarrow S_n$) measured using picosecond and femtosecond pump–probe experiments to those orientations calculated from the difference in angular orientation of the $S_0 \rightarrow S_n$ and $S_0 \rightarrow S_1$ transition moments determined from the steady-state fluorescence anisotropy measurements. We performed our investigation in the following two ways. First, we selected PDs which differ by the spectral position of the linear absorption band relative to the 532 nm pump beam. For PDs 2351, 2350, 2335 and 2338 the pump beam is within the $S_0 \rightarrow S_1$ band, for PDs 2257 and 824 – within the $S_0 \rightarrow S_2$ band and for PD 2332 – within the $S_0 \rightarrow S_3$ band. The probe beam of the same wavelength (532 nm) is absorbed by the $S_1 \rightarrow S_5$ transition as was determined from transition modeling of all the dyes.

Let us analyze the experimental data shown in Table 3. The largest anisotropy values 0.4 (theoretical limit) have been obtained for PDs 2350 and 2351 in ethylene glycol and slightly reduced values of 0.38 and 0.34 – in the ethanol solution. For PDs 2335 and 2338 anisotropy values are in the range 0.32–0.35, meaning that for the dyes excited directly into the $S_0 \rightarrow S_1$ band (or high vibrational levels of this band) the $S_1 \rightarrow S_5$ transition moment is oriented nearly parallel to the ground-state ab-

sorption dipole moment (<20°). The smallest anisotropy values 0.22–0.26 (and the largest angles 29–33°) have been obtained for PDs 824 and 2257 excited into the $S_0 \rightarrow S_2$ band, which correlates with the steady-state excitation anisotropy measurements. The intermediate values in anisotropy 0.28–0.3 have been obtained for PD 2332 excited into the $S_0 \rightarrow S_3$ band.

The second set of measurements was performed for PD 2338 using the femtosecond polarization resolved pump–probe setup as described in Section 2.2.3. We tested two excited-state absorption bands, the $S_1 \rightarrow S_5$ and the $S_1 \rightarrow S_2$ by pumping into the main absorption band $S_0 \rightarrow S_1$. Anisotropy values were measured at two time delays: 0.6 and 30 ps. We found that $R(t = 0.6\ \text{ps}) = 0.36$ and $R(t = 30\ \text{ps}) = 0.32$ for both transitions, see Fig. 8(a). That means that both the excited-state transitions are oriented almost parallel to each other as well as to the $S_0 \rightarrow S_1$ transition. A slight decrease in anisotropy from 0.36 to 0.32 is indicative of a ~3° reorientation during the 30 ps time delay. After that we tuned the pump wavelength to 380 nm ($S_0 \rightarrow S_4$ transition) and fixed the probe wavelength at 532 nm ($S_1 \rightarrow S_5$ transition). As can be seen from the steady-state excitation anisotropy measurements shown in Fig. 4(a), the $S_0 \rightarrow S_4$ transition forms the largest angle (~65°) with the ground-state dipole, therefore the anisotropy should be strongly affected. The pump–probe data is presented in Fig. 8(b). The calculated anisotropy value of $R(t = 30\ \text{ps}) = -0.1$, which means that the angle between $S_0 \rightarrow S_4$ and $S_1 \rightarrow S_5$ transition dipole moments is approximately 65°. The same angle was found for relative orientation of $S_0 \rightarrow S_1$ and $S_0 \rightarrow S_4$ transitions from steady-state measurements.

Thus, we can conclude that the two measurement techniques give the same results, indicating that after excitation the molecule's ultrafast relaxation processes do not appreciably change the transition dipole moment direction. From our point of view further work in this direction could lead to the development of a methodology, which can be applied to cases in which the steady-state measurements cannot be used, for example in cases of nonfluorescent molecules or solvents with low viscosity, etc.

However, we still do not fully understand several experimental results relating to the strength and orientation of the transitions. It is well known that the orientation of the transition dipole moment is determined by the wavefunctions of the states involved and the molecular structure. The symmetry of the PDs studied is C_{2V} (existence of the axis and plane of symmetry) leading to the symmetry representation of the energy states given in Fig. 4(b). The direction of the $S_0 \rightarrow S_n$ transition moment in the Parr–Pariser–Pople (PPP) quantum-chemical calculations, with the approximation of a symmetric charge distribution [4], may be parallel to polymethine chromophore principle axis ($S_0 \rightarrow S_1,\ S_0 \rightarrow S_3,\ S_0 \rightarrow S_5, \ldots$) or perpendicular to it ($S_0 \rightarrow S_2,\ S_0 \rightarrow S_4, \ldots$). Typically for PDs only the orientations of $S_0 \rightarrow S_1$ and $S_0 \rightarrow S_4$ transition moments are close to the calculated directions. Others show substantial differences. For example, for PD 2338 (Fig. 4(a)), the $S_0 \rightarrow S_5$ transition (parallel by calculations) is even more perpendicular than the $S_0 \rightarrow S_2$ transition. In the literature this disagreement is usually explained by invoking extra processes such as deformational and torsion vibrations in excitation, relaxation and emission processes [6]. The orientation of the $S_1 \rightarrow S_n$ transition calculated by standard AM1 and PPP quantum-chemical methods [4] is also shown in Fig. 4(b). According to the symmetry selection rules, the $S_1 \rightarrow S_2$ and the $S_1 \rightarrow S_4$ transitions should be allowed and oriented parallel to the $S_0 \rightarrow S_1$ transition, which is in agreement with the measurements. Transition $S_1 \rightarrow S_3$ was never observed experimentally. Transition $S_1 \rightarrow S_5$, which is responsible for the large broadband ESA in the visible region, should also be forbidden and oriented perpendicular to the $S_0 \rightarrow S_1$ transition according to the symmetry assignment. Therefore, we consider these results as an indication of strong symmetry breaking for the symmetric PDs that have a relatively long polymethine chromophore. Evidence for symmetry breaking in some PDs was discussed in [19], where "totally symmetric and nontotally symmetric" path mechanisms were proposed. Our understanding is that the development of a new approach in quantum-chemical calculations based on nontotally symmetric charge distributions in structurally symmetric PDs would

lead to an understanding of the strength and orientation for the $S_0 \rightarrow S_n$ and the $S_1 \rightarrow S_n$ transitions.

5. Conclusions

Picosecond and femtosecond polarization-resolved pump–probe measurements give a variety of information about lifetimes, molecular motions, anisotropy decays and transition orientations in different environments.

We have described a detailed investigation of a new series of PDs, which have attractive properties for optical limiting applications in liquid solutions and a polymeric host. From anisotropy decay data we found the rotation times in the solvents of different polarity and viscosity (ethanol, ethylene glycol and methylene chloride) and in an elastopolymer PUA. Reorientational decays in the solvents followed a single exponential behavior that is evidence for the allowed molecular motions leading to complete depolarization of the excited states. From the comparison of measured and calculated rotation times, we considered the solvent effects (''stick'' and ''slip'' rotation conditions). In contrast to liquid solutions, decays in PUA followed a double exponential behavior with two very different rotation times. The fast rotational component may be connected with the rotation of molecular fragments, which are limited by the free volume of microcavities. The slower rotational component is probably connected with the rotation of the entire molecule due to the faster segmental dynamics and microscale fluctuations of density in viscoelastic PUA.

We have analyzed the maximum anisotropy values in the nonlinear response of PDs, which made it possible to calculate the angles between the excited-state (probe) and ground-state (pump) transition. These results were compared to the steady-state fluorescence anisotropy measurements and good agreement was found between the experiments.

However several experimental results relating to the strength and orientation of the transitions still remain unanswered. We expect that the development of a new approach in quantum-chemical calculations based on nontotally symmetric charge distributions in structurally symmetric PDs would lead to progress in obtaining a deeper understanding of the nature of ESA transitions and to the prediction of the nonlinear optical properties of newly synthesized dyes.

Acknowledgements

This work was carried out under the support of the National Science Foundation (Grant No. 9970078), the Office of Naval Research (Grant No. N00014-97-1-0936), the Naval Air Warfare Center Joint Service Agile Program (Contract No. N00421-98-C-1327), the Air Force Office of Scientific Research (Grant No. F49620-93-C-0063), and The University of Florida MINSA program (Contract No. UFEIES0009001).

References

[1] J.H. Lim, O.V. Przhonska, S. Khodja, S. Yang, T.S. Ross, D.J. Hagan, E.W. Van Stryland, M.V. Bondar, Yu.L. Slominsky, Chem. Phys. 245 (1999) 79–97.
[2] M. Pittman, P. Plaza, M.M. Martin, Y.H. Meyer, Opt. Commun. 158 (1998) 201–212.
[3] M.H. Meyer, M. Pittman, P. Plaza, J. Photochem. Photobiol. A 114 (1998) 1–21.
[4] R.A. Negres, O.V. Przhonska, D.J. Hagan, E.W. Van Stryland, M.V. Bondar, Yu.L. Slominsky, A.D. Kachkovski, IEEE J. Selected Topics Quantum Electron. 7 (2001) 849–863.
[5] H.E. Lessing, A. Von Jena, Chem. Phys. Lett. 59 (1978) 249–253.
[6] A. Penzkofer, J. Wiedmann, Opt. Commun. 35 (1980) 81–86.
[7] O.V. Przhonska, D.J. Hagan, E. Novikov, R. Lepkowicz, E.W. Van Stryland, M.V. Bondar, Yu.L. Slominsky, A.D. Kachkovski, Chem. Phys. 273 (2001) 235–248.
[8] H.E. Lessing, A. Von Jena, Chem. Phys. Lett. 42 (1976) 213–217.
[9] H.E. Lessing, A. Von Jena, M. Reichert, Chem. Phys. Lett. 36 (1975) 517–522.
[10] A. Von Jena, H.E. Lessing, Chem. Phys. 40 (1979) 245–256.
[11] Yu.L. Slominsky, A.L. Smirnova, S.V. Popov, Ukr. Khim. Zh. 50 (1984) 638–640.
[12] F.A. Mikhailenko, N.P. Vasilenko, A.D. Kachkovski, Yu.J. Rozhinski, Zh. Org. Khim. 18 (1982) 435–441.
[13] A.I. Tolmachev, Yu.L. Slominskii, A.A. Ischenko, New cyanine dyes absorbing in the NIR region, in: Near-infrared Dyes for High Technology Applications, in: S.

Daehne, U. Resh-Genger, O.S. Wolfbeis (Eds.), NATO ASI Series, vol. 52, Kluwer Academic Publishers, Dordrecht, Boston, London, 1998, pp. 385–415.
[14] O. Przhonska, Applications in polymers, in: Near-Infrared Applications in Biotechnology, in: R. Raghavachari (Ed.), Practical Spectroscopy Series, vol. 25, Marcel Dekker, New York, 2000, pp. 235–262.
[15] R. Grigonis, A. Ischenko, G. Sinkevicius, Y.u. Slominsky, in: Lasers and Ultrafast Processes, 4, Vilnius University Press, 1991, pp. 197–199.
[16] J.R. Lakowicz, in: Principles of Fluorescence Spectroscopy, second ed., Kluwer Academic/Plenum Publishers, New York, 1999, p. 698.
[17] A. Dogariu, T. Xia, D.J. Hagan, A.A. Said, E.W. Van Stryland, J. Opt. Soc. Am. B 14 (1997) 796–803.
[18] R.L. Fork, C.V. Shank, C. Hirlimann, R. Yen, W.J. Tomlinson, Opt. Lett. 8 (1983) 1–4.
[19] A. Sanchez-Galvez, P. Hunt, M.A. Robb, M. Olivucci, T. Vreven, H.B. Schlegel, J. Am. Chem. Soc. 122 (2000) 2911–2924.